Estimation of accuracy, stiffness and stability of shell structures of mirror antennas using computer simulation

Andrii Sverstiuk[1,*,†], Mykola Stashkiv[2,†], Andrii Remez[2,†], Mykola Poshyvak[2,†] and Volodymyr Machohan[1,†]

[1] *I. Horbachevsky Ternopil National Medical University, Maidan Voli, 1, Ternopil, 46002, Ukraine*
[2] *Ternopil Ivan Puluj National Technical University, Rus'ka str. 56, Ternopil, 46001, Ukraine*

Abstract

The paper deals with simulation modeling of shell structures of mirror antennas in the evaluation of accuracy, stiffness, and stability. The relevance of the study lies in the fact that it is the loads on thin-walled elements of mirror antennas that determine their strength and durability, depending on the purpose and method of operation of the device of which the antenna is an integral part. Attention is focused on loads that can be of different types and are determined mainly by mechanical effects and temperature conditions, as well as on the shell elements of DSA structures, which are made in the form of shells of complex shape. When assessing the strength and serviceability of shell structures, the problems of stress-strain state, stability, and bearing capacity in static and dynamic formulations are considered. The basic concepts, principles of satellite dishes functioning, and results of local stability study are considered. The method of realization of the formation of a reinforced composite material and the method of electric arc spraying of mesh material are described. Attention is focused on the mutual fixation of the sputtered material and thermal loads. The basic equations of the stress-strain state of the shells and the results of simulation modeling of wind loading are presented. A graphical representation of the reinforced composite material, an antenna with a diameter of 1.5 m and a mesh aperture of 5 mm is presented. Simulation modeling of the heterogeneity of the distribution of the safety factor for a 3 mm thick aluminum antenna and the safety factor for a reinforced composite parabolic antenna is carried out. Separately, the results of modeling deformation processes in an antenna made of a solid sheet of aluminum under wind load are presented, which is extremely important for natural factors affecting the stability, reliability, and durability of the means of transmitting and receiving signals from satellites, especially in war conditions.

Keywords

antenna mirrors, electric arc spraying, reinforced composite material, stiffness, stress-strain state

CITI'2024: 2nd International Workshop on Computer Information Technologies in Industry 4.0, June 12–14, 2024, Ternopil, Ukraine
* Corresponding author.
† These authors contributed equally.
sverstyuk@tdmu.edu.ua (A. Sverstiuk); stashkiv@tntu.edu.ua (M. Stashkiv); filvasoxz@gmail.com (A. Remez); claruspuer01@gmail.com (M. Poshyvak); machohanvr@tdmu.edu.ua (V. Machohan)
0000-0001-8644-0776 (A. Sverstiuk); 0000-0002-7325-8016 (M. Stashkiv); 0009-0005-4846-4650 (A. Remez); 0009-0009-9655-4123 (M. Poshyvak); 0009-0003-1944-0161 (V. Machohan)

1. Introduction

The theory of shells has been developed quite fully and is presented in various works of scientists [1]. The source of its development is technical specifications. The main achievements of the theory are reflected in many works, of which we will highlight the manufacturing, production and design, which were carried out by scientists from Ukraine and foreign authors, as reflected in works [2, 3]. These papers describe the main achievements of the theory of shells, present the general equations of the theory and methods for solving them, and consider many special problems.

Determination of the stress-strain state (SSS) (forces and strains) of shell elements is usually not sufficient for their limit states, which characterize the performance of these elements. Achievement of the limit states may be associated with different mechanisms of destruction of structural elements. These issues are related to the study of the entire process of deformation of the system in a physically and geometrically complicated nonlinear formulation with the determination of the limit or crestal loads in one sense or another, characterizing the limit state of the system.

It is important to take into account the real properties of the material: plasticity, viscoelasticity, and creep. This significantly complicates the formulation and methods for solving the problems of stress-strain state and boundary states of shell systems (compared to elastic ones).

Certain simplifications are achieved by adopting some idealized models. For example, the load-bearing capacity of elastoplastic structures is sometimes considered on the basis of a model of a perfectly plastic body. The corresponding section of the theory of plasticity, the theory of limit equilibrium, discusses effective methods for determining the bearing capacity that can be applied to the calculation of many real systems.

2. Basic concepts and principles

A satellite antenna is an antenna used to receive or transmit radio signals between ground stations and artificial Earth satellites [4, 5]. Mirror antennas are the most common class of satellite dishes. They are used in different bands, from decimeter waves to Ku-band, and on different types of stations - from individual TV reception systems to space communication centers. Mirrored antennas are antennas in which the field in the opening is formed as a result of the reflection of an electromagnetic wave from the metal surface of a special reflector (mirror). The source of the electromagnetic wave is usually an antenna called a mirror irradiator or simply an irradiator. The mirror and the irradiator are the main elements of a mirror antenna. The surface of the mirror is shaped to form the desired radiation pattern (RP). The most common mirrors are in the form of a paraboloid of rotation, a truncated paraboloid, a parabolic cylinder, or a specially shaped cylinder. The irradiator is placed in the focus of the paraboloid or along the focal line of the cylindrical mirror [6] (Fig. 1).

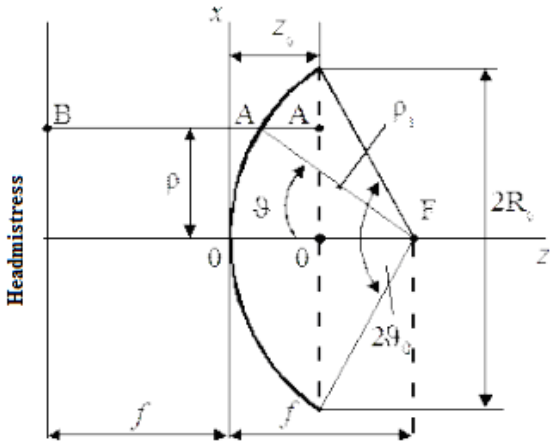

Figure 1: Geometrical characteristics of the paraboloid of rotation

From the definition of a parabola, its basic property follows: the sum of the distances from the focus F to any point A on the parabola and from this point A to point A' on the mirror's opening is constant $FA + AA' = const$. Due to this property, the optical paths from the focus to the opening points are identical, so that a spherical wave created by a point illuminator placed in the focus is converted into a plane wave after reflection from the paraboloid of rotation. Accordingly, a cylindrical wave produced by a linear irradiator is converted into a plane wave by a parabolic cylinder. In both cases, the field on the radiating surfaces of the parabolic antennas is in phase, which achieves high radiation directivity. There are two types of parabolic antennas: direct-focus (Fig. 2) and offset (Fig. 3).

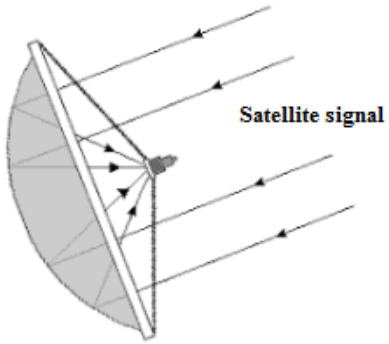

Figure 2: View of a direct-focus antenna

The direct-focus antenna is a classical rotation parabolic antenna. This allows for a more accurate orientation to the selected satellite. Typically, such antennas are used to receive a signal in the C-band, which is weaker than the signal in the Ku-band. However, it is also possible to receive a signal in the Ku-band, as well as a combined signal.

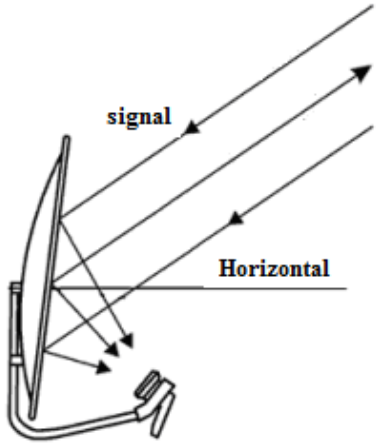

Figure 3: View of the offset antenna

The offset antenna is the most common in individual satellite TV reception. An offset antenna is an elliptical paraboloid (in the cross-section of an ellipse). The focus of such a segment is located below the geometric center of the antenna, which eliminates shadowing of the antenna's useful area by the irradiator and its supports, which increases its efficiency with the same mirror area as an axisymmetric antenna. Typically, offset antennas are used to receive Ku-band signals (in linear and circular polarization). However, it is also possible to receive a signal in the C-band, as well as a combined signal [7].

In the course of operation, under the influence of mechanical loads or temperature field, structural elements may acquire imperfections: imperfect shapes, changes in material characteristics, such as hardening, etc. Such imperfections also occur during the manufacturing process of structures. They must be taken into account when calculating the stress-strain state and especially the ultimate loads, since imperfections resulting from various causes can reduce the load-bearing capacity of the structure. At the same time, special types of imperfections (e.g., for the shell - if they do not coincide with the form of exhaustion of its bearing capacity) do not reduce and, in principle, can slightly increase the bearing capacity of some shell elements. Therefore, the issue of accounting for initial imperfections is of great importance. It becomes even more complicated for elastic-plastic shell systems, where not only the effect of changes in the initial shape of the shell is important, but also the effect of the loading history (in particular, changes in material properties during loading). Some issues of studying the shape imperfections and residual stresses on the bearing capacity of shells are considered in the paper.

Below is the basic information about mechanical loads acting on thin-walled elements of the SFA in various cases of their operation. Some problems of thermal conductivity are considered, which allow determining the temperature field in shells of complex shapes. The basic information of the theory of shells is presented, which is used to develop algorithms for calculating the stress-strain state of shells of complex shape, which are elements of thin-walled SAS.

It was noted above that in certain cases the performance of the antenna shell elements is determined by the loss of stability.

Methods for solving problems in the theory of shells are described in the above-mentioned and other publications. Effective methods for solving the problems of stability and oscillations of shells were developed in [8].

The results of the study of the local stability (statics and dynamics) of one of the elements of the SAR: a mirror in the form of a spherical segment under an edge local impact are presented below.

3. Method for implementing the formation of a reinforced composite material

Formation of shells by electric arc spraying and application of composite material. The formation of mirror antennas consists of several stages. The first stage is the deformation of a two-dimensional mesh and the fixing of nodes by electric arc spraying with aluminum [9] (Fig. 4).

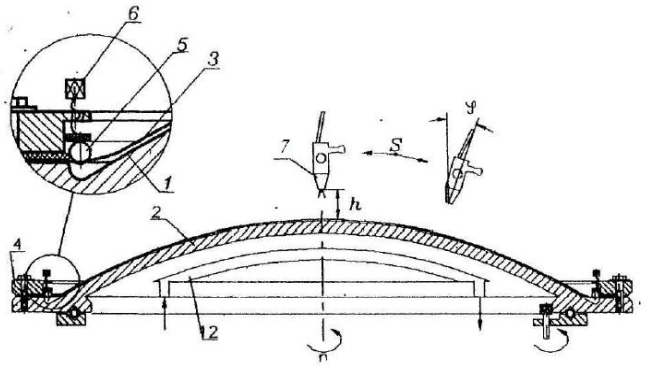

Figure 4: Electric arc spraying method for mesh material

The mesh blank 3 is placed on the working surface of the punch and its edges are secured with a clamp 4. A pre-made rim 5 is placed on the surface of the mesh blank along the contour of the punch and moved, for example, with elastic clamps 6, in a direction that ensures that the blank is crimped on the working surface of the punch. In the manufacture of large-sized shells, one or more additional mesh blanks with larger meshes and made of wire of a larger diameter are applied to the first blank with small meshes. The workpiece made of mesh material formed from a wire of small diameter d (Fig. 5), applied to the working surface of the punch, practically under the action of its own weight, takes the form of the working surface of the punch, as free mutual displacement of wires 7 and 8 in nodes 9 is ensured. The next step is the operation of coating the workpiece, which is performed, for example, using an electric arc or plasma sprayer 10 (Fig. 4). In this case, the end of the outlet nozzle of the sprayer is set at a distance h to the surface of the workpiece, and the axis of the arc torch is normal to the surface of the workpiece. The mutual movement of the punch and the nozzle of the spray gun or several spray guns during their parallel operation (for example, rotation with a variable angular velocity n of the punch 2 together with the workpiece 3 and radial feeding S of the spray gun 10 with its

corresponding angular displacementϕ depending on the coordinate of the spraying zone) is taken to ensure uniformity of the coating layer over the entire surface of the workpiece. The shape of the torch and the nature of the distribution of the sprayed material and temperature over its volume (which can be controlled, for example, by changing the air pressure P that forms the torch and the wire drawing speed when using electric arc spraying), the linear speed of the relative movement of the sprayer relative to the workpiece, the distance h to the workpiece and the number of passes of one spraying zone determine the time during which the mutual fixation of the sprayed material 11 (Fig. 7) of the wires 7 and 8 in all the same type nodes 9 of the mesh workpiece and the specified values a_1 and b_1 of the average mesh sizes (Fig. 6) or the time for complete closure of the mesh meshes and formation of a continuous surface of the shells are achieved.

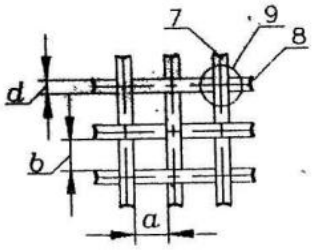

Figure 5: Mesh material with a diameter of d

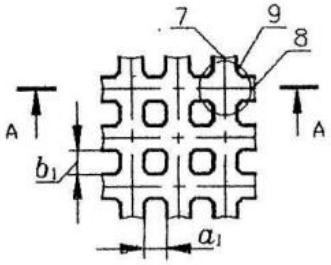

Figure 6: Average mesh size after spraying

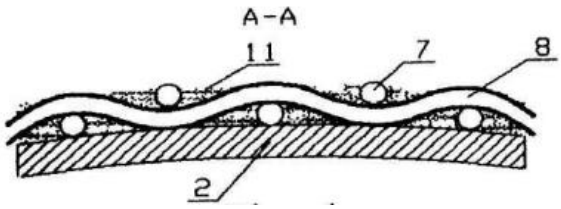

Figure 7: Mutual fixation with sprayed material

The second stage after spraying on the punch is to obtain a surface with a high temperature and apply a composite material such as polystyrene. Polystyrene is a polymeric material used in the manufacture of various products due to its unique properties. As a result, we obtained a shell surface that can be called a reinforced composite material [10, 11].

3.1. Thermal loads

Let's consider the temperature fields of the fuel cells made as shells. The most typical influence that causes such fields is solar radiation. Some works indicate methods for determining temperature fields in structures [12, 13, 14].
The heat balance equation has the form:

$$\alpha_c q_s F = \alpha_e \sigma T^4 F_e \qquad (1)$$

where $\alpha_c, a_в, \sigma$ are the absorption (emission) coefficients of solar and own thermal radiation, radiation of an absolutely black body; q_s is the solar constant, $q_s = 1400 Bm/м^2$; F_0 is the projection of the illuminated part of the surface to the direction of solar radiation; $F_в$ is the total surface of own heat radiation.
From (1), let's find the average temperature:

$$T = \left(\frac{\alpha_c}{\alpha_в} \cdot \frac{q_s}{\alpha} \cdot \frac{F_o}{F_в} \right)^{\frac{1}{4}} \tag{2}$$

It should be noted that a number of papers contain information on the spectral nature of all radiation characteristics, the nature of wave propagation at the interface between two media, reflection and absorption of waves from different media (metals, dielectrics, etc.).

The parameters of thermal fields depend on the refractive, absorptive, and emissive coefficients (the degree of blackness of the material). They are interrelated and depend on the electrical and magnetic constants of the material. It should be noted that the temperature fields in shell structures arbitrarily oriented with respect to the direction of the rays have not been studied.

Assuming that the antenna mirror is made in the form of a shell, consider a rotating shell on which a parallel stream of solar radiation falls $q_s r(t)$.
According to the heat balance equation for a solid volume element (a consequence of the first law of thermodynamics, the law of conservation of energy), the change in the total heat flux in the volume element due to heat conduction q_c , radial transfer q_r , and an increase in thermal energy (enthalpy) is zero:

$$div\left[q_c + q_r\right] + \rho c_p T_t = 0 \tag{3}$$

where c_p and ρ are the specific heat capacity and density of the medium; and q_r are described above.

When calculating the radiation transfer, individual monochromatic electromagnetic waves of a given frequency are usually considered ω . It is convenient to operate with the frequency rather than the wavelength l, since the latter changes its value when radiation passes from one medium to another. Denoting the spectral absorption coefficient $\chi(\omega)$ as the inverse of the average free path length of a photon $\lambda_p = \frac{1}{\chi_\lambda}$, consider an optically thick (opaque) medium when the optical thickness $\tau_{0\omega} = \frac{H}{\lambda_p} \gg 1$.

The radiating medium can be considered as a continuum of photons. In this case, it is assumed that each element of the medium, as in the case of molecular conductivity, is influenced only by neighboring elements. Under such conditions, the transfer of radiation energy in the medium can be equated to diffusion transfer [15].

The spectral flux of radiation in this case is represented as:

$$q_{r\omega} = -\frac{4\pi}{3x(\omega)} \nabla I_{\omega b}(T) \tag{4}$$

where $I_{\omega b}(T)$ is described by the Planck radiation formula:

$$I_{\omega b}(T)=\frac{2h\omega^3 n^2}{c_o^2\left[\exp\frac{h(\omega)}{KT}-1\right]}=\lim\left[\frac{dE_\omega}{dF\cos\gamma}d\Omega d\omega dt\right] \quad (5)$$

Here $K = 1{,}38\cdot 10^{-32}$ J/K is the Boltzmann constant: $h = 6{,}625\cdot 10^{-34}$ J/s is Planck's constant; $n(\omega)$ is the refractive index of the medium; is the speed of light in a vacuum; T is the absolute temperature; ∇ is a gradient symbol.

3.2. Basic equations of the stress-strain state of shells

The equations describing the deformation of a shell under load include equilibrium equations, relations that relate deformations and displacements, and physical relations. The first two groups of equations are applicable to describe the state of various shells regardless of the model of shell behavior used.

Shell behavior models are accounted for by the third group of equations - physical relations. These models are determined by the properties of the material from which the shell is made (elasticity, plasticity, viscoelasticity, creep, etc.).

The equations describing the deformation of shells differ depending on the class of problems considered (stress-strain state, stability, fracture, etc.), the class of shells (shape, structure), the type of loading (statics, dynamics, temperature effects), and accuracy requirements [16].

Let us consider a deformable solid body and introduce a curved orthogonal coordinate system for it . The total displacement of a point of the body is characterized by a vector whose projections on the coordinate lines are denoted by $u_\alpha, u_\beta, u_\gamma$. Let us write the general relations expressing deformations and displacements in terms of the so-called Lamé coefficients H_i (i = 1, 2, 3), which relate the increase in the arcs of the coordinate lines to the increase in the corresponding curved coordinates:

$$\begin{aligned}
e_{\alpha\alpha}&=\frac{1}{H_1}u_{\alpha,\alpha}+\frac{1}{H_1H_2}H_{1,\beta}u_\beta+\frac{1}{H_1H_3}H_{1,\gamma}u_\gamma,\\
e_{\beta\beta}&=\frac{1}{H_2}u_{\beta,\beta}+\frac{1}{H_2H_3}H_{2,\gamma}u_\gamma+\frac{1}{H_1H_2}H_{2,\alpha}u_\alpha,\\
e_{\gamma\gamma}&=\frac{1}{H_3}u_{\gamma,\gamma}+\frac{1}{H_1H_3}H_{3,\alpha}u_\alpha+\frac{1}{H_2H_3}H_{3,\beta}u_\beta,\\
e_{\alpha\beta}&=\frac{H_1}{H_2}\left(\frac{1}{H_1}u_\alpha\right)_\beta+\frac{H_2}{H_1}\left(\frac{1}{H_2}u_\beta\right)_\alpha,\\
e_{\beta\gamma}&=\frac{H_2}{H_3}\left(\frac{1}{H_2}u_\beta\right)_\gamma+\frac{H_3}{H_2}\left(\frac{1}{H_3}u_\gamma\right)_\beta,\\
e_{\gamma\alpha}&=\frac{H_3}{H_1}\left(\frac{1}{H_3}u_\gamma\right)_\alpha+\frac{H_1}{H_3}\left(\frac{1}{H_1}u_\alpha\right)_\gamma
\end{aligned} \quad (7)$$

Deformations $e_{\alpha\alpha}, e_{\beta\beta}, e_{\gamma\gamma}$ characterize the elongation of linear elements parallel to the axes ; deformations $e_{\alpha\beta}, e_{\beta\gamma}, e_{\gamma\alpha}$ - shifts - changes in the initially right angle between linear elements. Shell - a body with two dimensions much larger than the third. Consider a single-layer shell. Let's introduce a median surface, the position of a point on which is determined by the Gaussian curvilinear coordinates α, β along the thickness of the shell - the z coordinates. When using the equation of coordinate (7) in the theory of shells, the Lamé coefficients $H_i = A_i(1 + k_i t)\left(i = 1,2; H_3 = 1, k_i = \frac{1}{R_i}\right)$ are related by the Codazzi-Gauss relations [16]:

$$\begin{aligned} &\left(\frac{1}{A_1}A_{2,\alpha}\right)_\alpha + \left(\frac{1}{A_2}A_{1,\beta}\right)_\beta = -k_1 k_2 A_1 A_2, \\ &\left(A_2 k_2\right)_\alpha = k_1 A_{2,\alpha}, \left(A_1 k_1\right)_\beta = k_2 A_{1,\beta} \end{aligned} \tag{8}$$

The theory of shells is traditionally based on a number of pleading hypotheses. According to the Kirchhoff-Love hypothesis, straight fibers of a shell normal to the median surface remain straight and normal to it after deformation. According to the Timoshenko hypothesis, the first condition is weakened: it is assumed that after deformation, these fibers remain straight and not perpendicular to the median surface, while the second condition remains the same. The introduction of the first of these hypotheses greatly simplifies the relation (7). In this case:

$$e_{\gamma\gamma} = e_{\beta\gamma} = e_{\alpha\beta} = 0 \tag{9}$$

The displacements of any of the shell layers located at a distance z from the median surface are determined as follows:

$$u_\alpha = u + z\theta_\alpha, u_\beta = v + z\theta_\beta, u_\gamma = \omega \tag{10}$$

where $\theta_\alpha, \theta_\beta$ are the angles of rotation of the median surface of the plane $\beta = const, \alpha = const, \theta_\alpha = -\frac{1}{A_1}\omega_a + uk_1, \theta_\beta = -\frac{1}{A_2}\omega_\beta + vk_2, k_i = R_i^{-1}$, R_i are the principal radii of curvature.

Relationships (10) are written on the assumption that elongations and displacements can be neglected compared to unity.

The deformations of these shell layers are defined as follows [17]:

$$\begin{aligned} e_{\alpha\alpha} &= e_\alpha = \varepsilon_\alpha + z\chi_\alpha, \\ e_{\beta\beta} &= e_\beta = \varepsilon_\beta + z\chi_\beta, \\ e_{\alpha\beta} &= \varepsilon_{\alpha\beta} + 2z\chi_{\alpha\beta} \end{aligned} \tag{11}$$

Here $\varepsilon_\alpha, \varepsilon_\beta, \varepsilon_{\alpha\beta}, \chi_\alpha, \chi_\beta, \chi_{\alpha\beta}$ - deformations and changes in the curvature of the median surface, presented in the form:

$$
\begin{aligned}
\varepsilon_\alpha &= \frac{1}{A_1}u_\alpha + \frac{1}{A_1A_2}A_{1,\beta}\upsilon + k_1\omega + \frac{1}{2}\left(k_1u - \frac{1}{A_1}\omega_\alpha\right)^2;\\
\varepsilon_\beta &= \frac{1}{A_2}u_\beta + \frac{1}{A_1A_2}A_{2,\alpha}u + k_2\omega + \frac{1}{2}\left(k_2\upsilon - \frac{1}{A_2}\omega_\beta\right)^2;\\
\varepsilon_{\alpha\beta} &= \frac{A_1}{A_2}\left(\frac{u}{A_1}\right)_\beta + \frac{A_2}{A_1}\left(\frac{\upsilon}{A_2}\right)_\alpha + \left(k_1u - \frac{1}{A_1}\omega_\alpha\right)\cdot\left(k_2\upsilon - \frac{1}{A_2}\omega_\beta\right);\\
\chi_\alpha &= \frac{1}{A_1}\left(\frac{1}{A_1}\omega_\alpha\right)_\alpha - \frac{1}{A_1A_2^2}A_{1,\beta}\omega_\beta + k_{1,\alpha}\frac{\upsilon}{A_2} + k_{1,\beta}\frac{\upsilon}{A_1} - k_1^2\omega;\\
\chi_\beta &= -\frac{1}{A_2}\left(\frac{1}{A_2}\omega_\beta\right)_\beta - \frac{1}{A_1^2A_2}A_{2,\alpha}\omega_\alpha + k_{2,\beta}\frac{\upsilon}{A_2} + k_{1,\alpha}\frac{u}{A_1} - k_2^2\omega;\\
\chi_{\alpha\beta} &= -\frac{2}{A_1A_2}\left(\omega_{\alpha\beta} - \frac{1}{A_1}A_{1,\beta}\omega_\alpha - \frac{1}{A_2}A_{2,\alpha}\omega_\beta\right) + (k_1 - k_2)\left[\frac{A_1}{A_2}\left(\frac{u}{A_1}\right)_\beta - \frac{A_2}{A_1}\left(\frac{\upsilon}{A_2}\right)_\alpha\right]
\end{aligned}
\tag{12}
$$

The equilibrium equations and boundary conditions are obtained on the basis of the variational principle of possible displacements of La Grange, according to which for equilibrium systems the sum of the work of external and internal forces is zero, i.e.

$$\delta\exists - \delta A_1 - \delta A_2 = 0 \tag{13}$$

where $\delta\exists$ is the variation of the work of internal forces; δA_1 is the work of external forces applied to the shell surface δA_2 is the variation of the work of external contour forces.

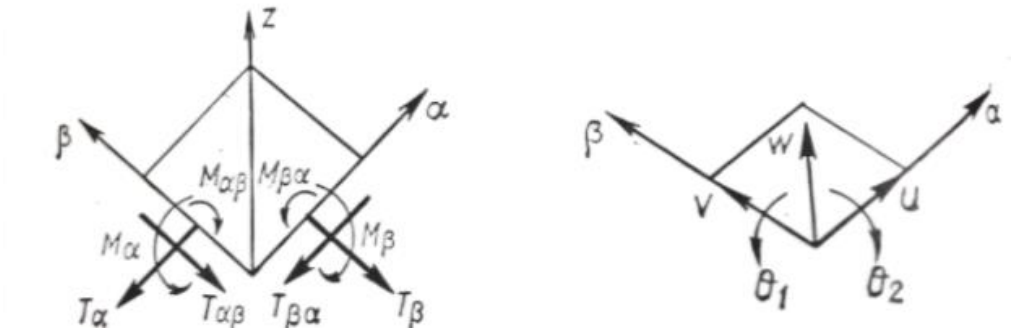

Figure 8: Decomposition of forces and moments

Let the shell be bounded by an edge contour L, consisting of parts L_1 and L_2, for which $\alpha = const$ and . KL_i are subjected to edge normal T_i^0 shear $T_{\alpha\beta}^0$ forces, intersecting forces Q_i^0 and bending moments M_i^0 (Fig. 8). In addition, the displacements of the points of the median surface $u^0, \upsilon^0, \omega^0$ and the angle of rotation θ^0 can be set on L_i . The surface of the shell S bounded by the contour is subjected to the loads distributed by the surface

q_1, q_2, q_z . The normal and tangential stresses in the cross-sections of the shell are denoted by $\sigma_\alpha, \sigma_\beta, \sigma_{\alpha\beta}$. Then $\delta\exists, \delta A_1, \delta A_2$ will be expressed as follows [18]:

$$\begin{aligned}
&\delta A_1 = \int_F \left(q_1\delta u + q_2\delta\upsilon + q_z\delta\omega\right) A_1A_2 d\beta,\\
&\delta A_2 = \int_{\Gamma_1} \left(T_\alpha^0\delta u + T_\alpha^0\delta\upsilon + Q_\alpha^0\delta\omega + M_\alpha^0\delta\theta_1\right) A_2 d\beta +\\
&+\int_{\Gamma_2} \left(T_{\beta\alpha}^0\delta u + T_\beta^0\delta\upsilon + Q_\beta^0\delta\omega + M_\beta^0\delta\theta_2\right) A_1 d\alpha,\\
&\delta\boxminus = \int_V \left(\sigma_\alpha\delta e_\alpha + \sigma_\beta\delta e_{\beta\beta} + \sigma_{\alpha\beta}\delta e_{\alpha\beta}\right) H_1H_2 d\beta_2 dz
\end{aligned} \tag{14}$$

Instead of voltages, let's introduce their corresponding integral characteristics-forces: normal:

$$\begin{aligned}
T_\alpha &= \int \sigma_\alpha \left(1 + zk_2\right) dz,\\
T_\beta &= \int \sigma_\beta \left(1 + zk_1\right) dz,\\
T_{\alpha\beta} &= \int \sigma_{\alpha\beta} \left(1 + zk_2\right) dz,\\
T_{\beta\alpha} &= \int \sigma_{\beta\alpha} \left(1 + zk_1\right) dz;
\end{aligned}$$

tangents:

$$\begin{aligned}
T_{\alpha\beta} &= \int \sigma_{\alpha\beta} \left(1 + kz_2\right) dz,\\
T_{\beta\alpha} &= \int \sigma_{\alpha\beta} \left(1 + zk_1\right) dz;
\end{aligned}$$

shear forces:

$$\begin{aligned}
Q_\alpha &= \int \sigma_{\alpha\beta} \left(1 + zk_2\right) dz,\\
Q_\beta &= \int \sigma_{\alpha\beta} \left(1 + zk_1\right) dz;
\end{aligned}$$

bending and torsional moments:

$$\begin{aligned}
M_\alpha &= \int \sigma_\alpha \left(1 + zk_2\right) zdz,\\
M_\beta &= \int \sigma_\beta \left(1 + zk_1\right) zdz,\\
M_{\alpha\beta} &= \int \sigma_{\alpha\beta} \left(1 + zk_2\right) zdz,\\
M_{\beta\alpha} &= \int \sigma_{\alpha\beta} \left(1 + zk_1\right) zdz;
\end{aligned}$$

Here, the integration is carried out within the range (-h/2, h/2); values of zk; less than one are neglected.

Substituting expression (14) into (13), we obtain:

$$\delta \exists = \int_S \left(T_\alpha \delta \varepsilon_\alpha + T_\beta \delta \varepsilon_\beta + S \delta \varepsilon_{\alpha\beta} + M_\alpha \delta \chi_\alpha + M_\beta \delta \chi_\beta + 2 M_{\alpha\beta} \delta \chi_{\alpha\beta} \right) A_1 A_2 d\alpha d\beta \tag{15}$$

Let us recall the Green's formula:

$$\int_S \varphi \psi_a d\alpha d\beta = \int_{\Gamma_1} \varphi \psi d\beta - \int_S \psi \varphi_\alpha d\alpha d\beta \tag{16}$$

Substituting expressions (14), (15) into (13) and using (16), we obtain the variational equation after the transformations:

$$N_1^0 + N_2^0 = \int_S \left(N_3 + A_1 A_2 q_z \right) \delta\omega d\alpha d\beta,$$

where

$$N_1^0 = \int_{\Gamma_1} \Big[\left(T_\alpha - T_\alpha^0 \right) \delta u + \left(S + 2k_2 M_{\alpha\beta} - M_{\alpha\beta}^0 \right) \delta\upsilon +$$
$$+ \left(Q_\alpha + \frac{1}{A_2} M_{\alpha\beta,\beta} - Q_\alpha^0 \right) \delta\omega + \left(M_\alpha - M_\alpha^0 \right) \delta\vartheta_1 \Big] A_2 d\beta - \int_S \left(N_1 + A_1 A_2 q_\alpha \right) \delta u d\alpha d\beta;$$

$$N_2^0 = \int_{\Gamma_2} \Big[\left(T_\beta - T_\beta^0 \right) \delta\upsilon + \left(S + 2k_1 M_{\alpha\beta} - M_{\alpha\beta}^0 \right) \delta u + \tag{17}$$
$$+ \left(Q_\beta + \frac{1}{A_1} M_{\alpha\beta,\alpha} - Q_\beta^o \right) \delta\omega + \left(M_\beta - M_\beta^0 \right) \delta\upsilon_2 \Big] A_1 d\alpha - \int_S \left(N_2 + A_1 A_2 q_\beta \right) \delta\upsilon d\alpha d\beta;$$

$$N_1 = \left(A_2 T_\alpha \right)_\alpha + \frac{1}{A_1} \left(A_1^2 S \right)_\beta - A_{2,\alpha} T_\beta + \left(k_1 A_1 M_{\alpha\beta} \right)_\beta + A_{1,\alpha} k_2 M_{\alpha\beta} + k_1 A_1 A_2 Q_\alpha;$$

$$N_2 = \left(A_1 T_\beta \right)_\beta + \frac{1}{A_2} \left(A_2^2 S \right)_\alpha - A_{1,\beta} T_\alpha + \left(k_2 A_2 M_{\alpha\beta} \right)_\alpha + A_{2,\alpha} k_1 M_{\alpha\beta} + k_2 A_1 A_2 Q_\beta;$$

$$N_3 = \left(A_2 Q_\alpha \right)_\alpha + \left(A_1 Q_\beta \right)_\beta - A_1 A_2 \left(k_1 T_\alpha + k_2 T_\beta \right);$$

$$Q_\alpha A_1 A_2 = \left(A_2 M_\alpha \right)_\alpha + \frac{1}{A_1} \left(A_1^2 M_{\alpha\beta} \right)_\beta - A_{2,\alpha} M_\beta - A_1 A_2 \left(T_\alpha \theta_1 + S\theta_2 \right);$$

$$Q_\beta A_1 A_2 = \left(A_1 M_\beta \right)_\beta + \frac{1}{A_2} \left(A_2^2 M_{\alpha\beta} \right)_\alpha - A_{1,\beta} M_\alpha - A_1 A_2 \left(T_\beta \theta_2 + S\theta_1 \right)$$

Since , $\delta\upsilon, \delta\omega, \delta\theta_1, \delta\theta_2$, are independent in the domain S and on the contours G_1, G_2, the equilibrium equations follow from the general variational equation:

$$\begin{aligned} N_1 + A_1 A_2 q_q &= 0, \\ N_2 + A_1 A_2 q_\beta &= 0, \\ N_3 + A_1 A_2 q_z &= 0 \end{aligned} \tag{18}$$

and boundary conditions:

$$
\begin{aligned}
&T_\alpha = T_\alpha^0,\\
&S + 2k_2 M_{\alpha\beta} = T_{\alpha\beta}^0,\\
&Q_\alpha + \frac{1}{A_2} M_{\alpha\beta,\alpha} = Q_\alpha^0,\\
&M_\alpha = M_\alpha^0,\\
&Q_\beta + \frac{1}{A_1} M_{\alpha\beta,\beta} = Q_\beta^0.
\end{aligned}
$$

The Lamé coefficients A_1, A_2 and curvatures k_1, k_2 for the most commonly used shells as structural elements are as follows [19]:
for a cylindrical shell:

$$
\begin{aligned}
&A_1 = 1,\\
&A_2 = R,\\
&k_1 = 0,\\
&k_2 = \frac{1}{R};
\end{aligned}
$$

for a spherical shell:

$$
\begin{aligned}
&A_1 = R,\\
&A_2 = R\sin\theta,\\
&k_1 = k_2 = \frac{1}{R};
\end{aligned}
$$

for conical shells:

$$
\begin{aligned}
&A_1 = 1,\\
&A_2 = r_0 + s\cos\beta,\\
&k_1 = 0,\\
&k_2 = \sin\frac{\sin\beta}{A_2};
\end{aligned}
$$

for the torus shell:

$$A_1 = R,$$
$$A_2 = d + R\sin\theta,$$
$$k_1 = \frac{1}{R},$$
$$k_2 = \frac{\sin\theta}{A_2};$$

4. Visualization

4.1. Results of wind load modeling

The normal wind load (Pa) can be determined in the first approximation by the formula

$$W = k \times \rho \times V^2,$$

where: k - drag coefficient (flow); ρ - air density, kg/m^3 (ρ = 1.225 kg/m^3); V is the wind speed, m/s.

According to the results of modeling (Figure 9) of the flow around a parabolic antenna with a diameter of 1.5 m [20] (made of a 3 mm thick aluminum sheet) by an incoming air flow with a speed of 20 m/s, a value of the normal wind load of ≈ 440 Pa was obtained, which corresponds to a flow coefficient k ≈ 0.9.

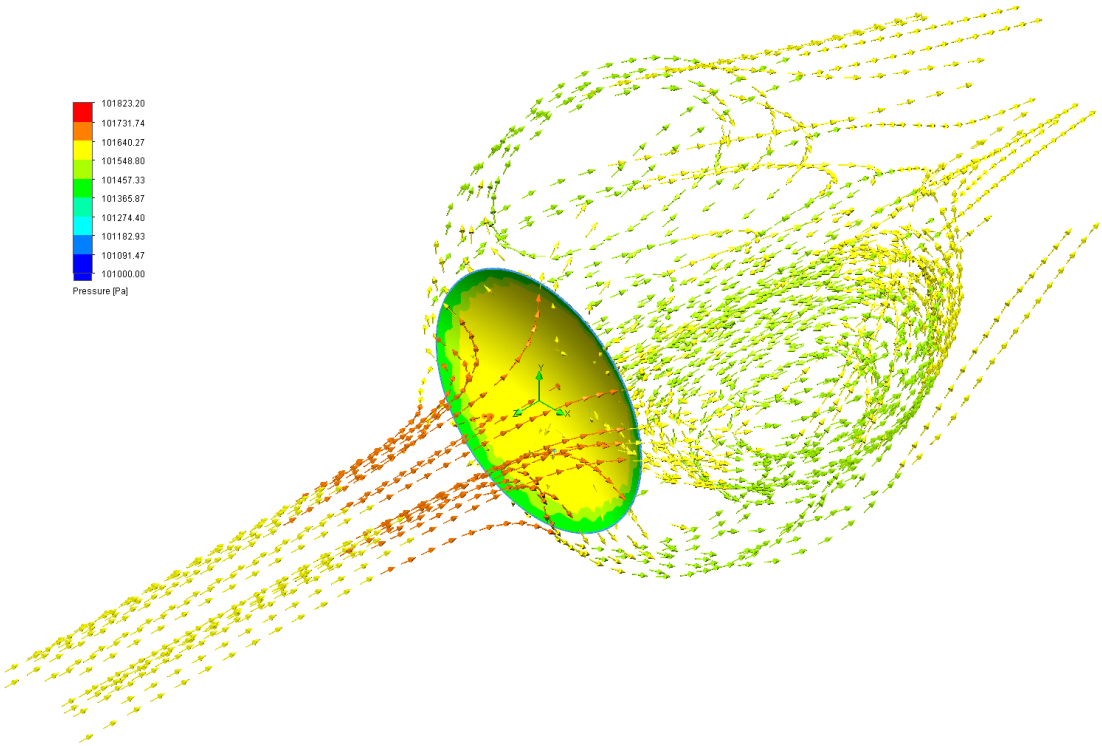

Figure 9: Wind load modeling

A solid-state model of a reinforced composite parabolic antenna consisting of the following elements was created (Figure 10, bottom to top):

- aluminum spraying;
- reinforcing mesh;
- protective plastic;
- ring of the locking mechanism.

4.2 Graphical representation of reinforced composite material

This is a 1.5-meter-diameter antenna model consisting of mesh material that has been electrodeposited and a composite layer overlaid on it Fig. 10.

Figure 10: Image of a 1.5 m diameter antenna with a 5 mm mesh aperture

To evaluate the stiffness-strength characteristics of antennas of solid and reinforced structures, we calculated their stress-strain state under the action of wind load and gravity Fig.11.

The calculation showed that despite the loss of stiffness of the reinforced structure antenna compared to the antenna made of a solid sheet of aluminum (105 kN/m vs. 664 kN/m), the safety factor of the reinforced structure antenna is 8.8 and remains sufficient, although it is significantly lower than that of the antenna made of a solid sheet of aluminum Fig. 12 and Fig.13.

The obtained thorough results on the evaluation of the accuracy, stiffness, and stability of the shell structures of mirror antennas using simulation modeling are the basis for their use in the instrumentation, radio engineering, and cyber-physical biosensor industries [21, 22, 23]. It should be noted that the rigidity of the antenna arrays affects the accuracy and quality of the transmitted information, but does not increase the speed.

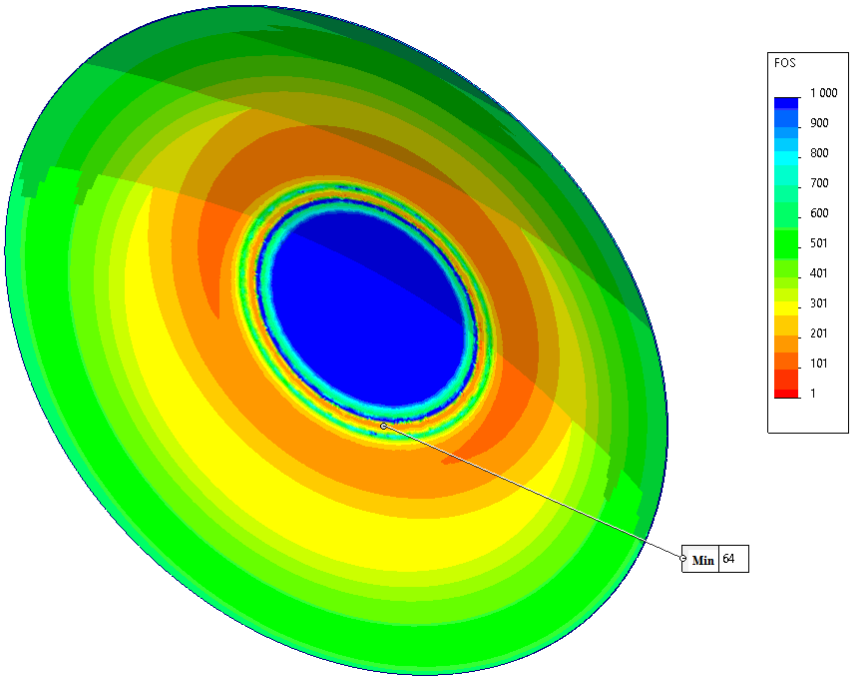

Figure 11: Safety factor for a 3 mm thick aluminum antenna

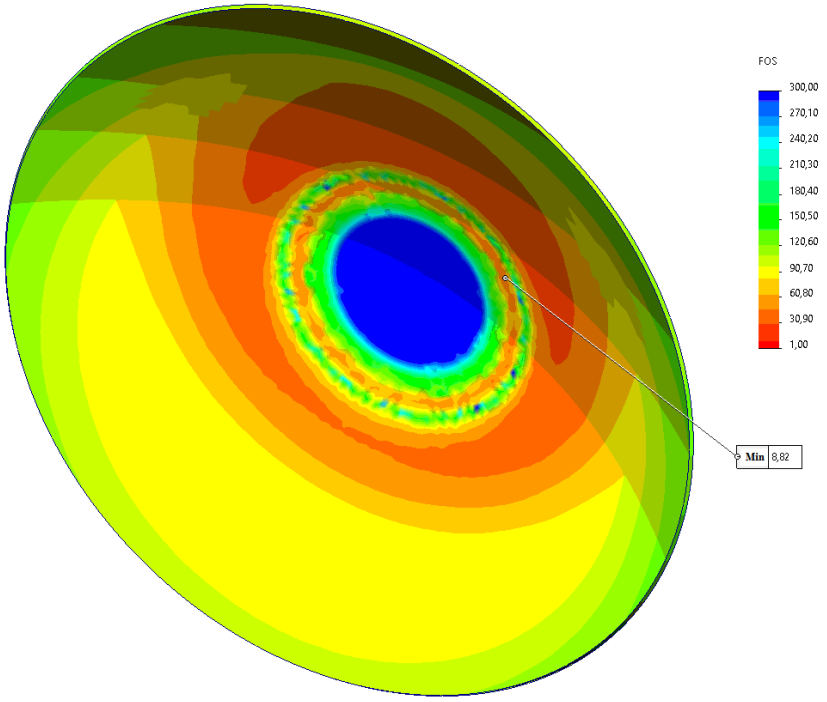

Figure 12: Safety factor for a reinforced composite parabolic antenna

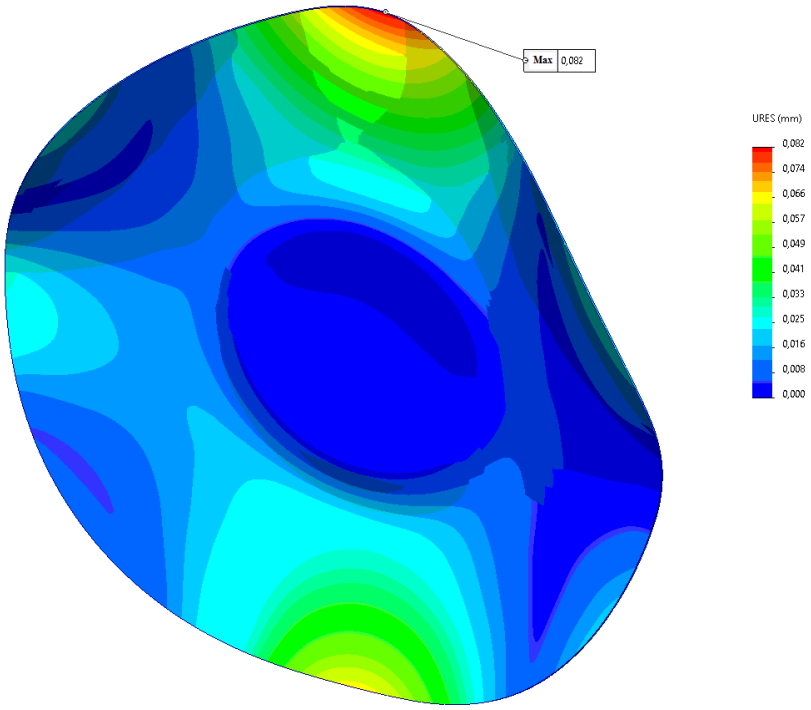

Figure 13: Deformation of an antenna made of a solid sheet of aluminum under wind load (scale of deformation display is 2000:1)

Conclusion

In the course of the work, the methods of manufacturing antenna systems and manufacturing reflective surfaces based on new technological and design ideas are considered. The process of formation of shells from mesh material that can be used for the manufacture of axisymmetric and non-axisymmetric reflectors or individual elements of mirror antennas is investigated.

This is because the formation of this material consists of several stages. The first stage is deformation of the two-dimensional mesh and fixing of the nodes by electric arc spraying with aluminum. The second stage, after sputtering on the punch, is to obtain a surface with a high temperature and apply a composite material such as polystyrene.

On the basis of calculations and graphs, that despite the loss of stiffness of the reinforced structure antenna compared to the antenna made of a solid sheet of aluminum (105 kN/m versus 664 kN/m), the safety factor of the reinforced structure antenna is 8.8 and remains sufficient, although it is significantly less than that of the antenna made of a solid sheet of aluminum.

References

[1] M. Palamar, I. Zelinskyy, M. Yavorska, The Device for Remote Measurements of Geometric Dimensions and Positions, Proceedings of the 2017 IEEE 9th International Conference on Intelligent Data Acquisition and Advanced Computing Systems: Technology and Applications (IDAACS), 21-23 September 2017, Bucharest, Romania. IEEE, Vol.1, pp. 524–527.

[2] M. Yavorska, T. Dubyniak, O. Manziy, S. Andreichuk, Study of the process and problems arising during the formation of shells by the method of electric arc spraying, MMMTES, Ternopil, November 22-23, 2022, pp. 85-87.
[3] V. Ovcharenko, S. Podlesny, S. Zinchenko, Fundamentals of the finite element method and its application in engineering calculations. Tutorial. Kramatorsk: 2008, 380 p.
[4] L. Khvostivska, M. Khvostivskyy, V. Dunetc, I. Dediv. Mathematical and Algorithmic Support of Detection Useful Radiosignals in Telecommunication Networks. Proceedings of the 2nd International Workshop on Information Technologies: Theoretical and Applied Problems (ITTAP 2022). Ternopil, Ukraine, November 22-24, 2022. P.314-318. ISSN 1613-0073.
[5] L. Khvostivska, M. Khvostivskyi, Dediv I., Yatskiv V., Palaniza Y. Method, Algorithm and Computer Tool for Synphase Detection of Radio Signals in Telecommunication Networks with Noises. CITI 2023. CEUR Workshop Proceedings. Ternopil, Ukraine, June 14-16, 2023. P.173-180. ISSN 1613-0073.
[6] G. Shulim, Fundamentals of mathematical theory of thermoelastic equilibrium of deformable solids with thin inclusions, Research and Publishing Center NTSh., Lviv, 2007. 715 p.
[7] T. Dubynyak, R. Dzhydzhora, O. Manziy, S. Andreichuk, The process of shells formation by electric arc spraying method and optimization by the criterion of their geometric shape accuracy, Scientific Journal of TNTU, Ternopil, 2021, Vol. 104, № 4, pp. 24-32.
[8] L. Matveeva The process of software development. From theory to practice, Kyiv, 2008,
402 p.
[9] V. Gudramovych, V. Skalskyi, Y. Selivanov, Holographic and acoustic-emission diagnostics of heterogeneous structures and materials: a monograph, Lviv, Prostir-M, 2017, 492 p.
[10] Z. Nazarchuk, Technical Diagnostics of Materials and Structures, in 8 volumes, Prostir-M, Lviv, 2018.
[11] Stukhlyak, P.D.; Buketov, A.V.; Panin, S.V.; Maruschak, P.O.; Moroz, K.M.; Poltaranin, M.A.; Vukherer, T.; Kornienko, L.A.; Lyukshin, B.A. Structural fracture scales in shock-loaded epoxy composites. Phys. Mesomech. 2015, 18, 58–74.
[12] D. Zaitsev, Mathematical Models of Discrete Systems, Primer. Odessa, 2004, 40 p.
[13] Konovalenko, I., Maruschak, P., Kozbur, H., Brezinová, J., Brezina, J., Nazarevich, B., Shkira, Y. Influence of Uneven Lighting on Quantitative Indicators of Surface Defects. Machines, 10 (3), art. no. 194 2022. doi: 10.3390/machines10030194.
[14] Konovalenko, I.; Maruschak, P.; Brezinová, J.; Prentkovskis, O.; Brezina, J. Research of U-Net-Based CNN Architectures for Metal Surface Defect Detection. Machines 2022, 10, 327.
[15] A. Karvatsky Finite element method in problems of mechanics of continuous media, Program implementation and visualization of results [Electronic resource], 2015,391 p.
[16] I. Tarapov, Continuum mechanics. Golden pages, Kharkov, 2002, 516 p.
[17] V. Dmitrieva, Physics, Kiev, Tehnika, 2008, 644 p.
[18] E. Hart, V. Hudramovich, Application of the projection-iterative scheme of the method of local variations to solving stability problems for thin-walled shell structures under localized actions, Strength Mater. 50, no. 6, 852-858, 2018.

[19] O. Zienkiewicz, R. Teylor, The Finite Element Method for Solid and Structural Mechanics, Elsevier, New York, 2005.
[20] A. Sinkovsky Materials for sawing and welding. Lecture notes for students. Lekts. Specialist. 7.092303 - technol. I statistical analysis of the development and improvement of the reliability of parts of machines and designs, Science and technology, 2008, 128 p.
[21] V.Martsenyuk, A. Sverstiuk, A. Klos-Witkowska, N.Kozodii, O. Bagriy-Zayats, I. Zubenko, Numerical analysis of results simulation of cyber-physical biosensor systems. CEUR Workshop Proceedings, 2019, 2516, pp. 149–164.
[22] Hankevych, V., Kyung, B., Tremblay, A.-M.S.: Weak ferromagnetism and other instabilities of the two-dimensional t–t′ Hubbard model at van Hove fillings. Phys. Rev. B 68, 214405 (2003)
[23] V. Martsenyuk, A. Sverstiuk, O. Bahrii-Zaiats, A. Kłos-Witkowska, Qualitative and Quantitative Comparative Analysis of Results of Numerical Simulation of Cyber-Physical Biosensor Systems. (2022) CEUR Workshop Proceedings, 3309, pp. 134 – 149.